Journal of Solid State Chemistry 184 (2011) 2744–2750

Contents lists available at SciVerse ScienceDirect

Journal of Solid State Chemistry

journal homepage: www.elsevier.com/locate/jssc

Transport and optical properties of heavily hole-doped semiconductors $BaCu_2Se_2$ and $BaCu_2Te_2$

Michael A. McGuire*, Andrew F. May, David J. Singh, Mao-Hua Du, Gerald E. Jellison

Oak Ridge National Laboratory, Oak Ridge, TN 37831, USA

ARTICLE INFO

Article history:
Received 15 June 2011
Received in revised form
10 August 2011
Accepted 14 August 2011
Available online 24 August 2011

Keywords:
$BaCu_2Te_2$
$BaCu_2Se_2$
Copper chalcogenide
Transport properties
Optical properties
Band structure

ABSTRACT

Experimental and theoretical studies of the electronic and optical properties of orthorhombic $BaCu_2Se_2$ and $BaCu_2Te_2$ are reported. Experimental data include the electrical resistivity, Hall coefficient, Seebeck coefficient, thermal conductivity, and lattice constants for $T \leq 300$ K, and optical transmission and diffuse reflectance data at room temperature. Nominally stoichiometric, polycrystalline samples form with hole concentrations inferred from Hall measurements of 2×10^{18} and 5×10^{19} cm^{-3} near room temperature for the selenide and telluride, respectively. The corresponding mobilities are near 15 $cm^2 V^{-1} s^{-1}$ for both materials. Optical measurements reveal a transition near 1.8 eV in $BaCu_2Se_2$, while no similar feature was observed for $BaCu_2Te_2$. First principles calculations indicate both materials are direct or nearly direct gap semiconductors with calculated gaps near 1.0 eV and 1.3 eV for the telluride and selenide, respectively, and predict weak absorption below about 2 eV. Transport properties calculated from the electronic structure are also presented.

1. Introduction

Multinary copper chalcogenides have complex and interesting solid state chemistries and physical properties, and have made significant impact in energy applications as some of the leading photovoltaic materials. Copper chalcogenides account for two of the most efficient photovoltaic materials: $CuIn_{1-x}Ga_xSe_2$, abbreviated CIGS [1], and $Cu_2ZnSn(S/Se)_4$ adopting the kesterite structure [2]. The crystal structures of CIGS and kesterites, as well as another leading photovoltaic material, CdTe, can be viewed as superstructures of the prototypical photovoltaic, silicon. We have been recently investigating the potential of more complex, Zintl-like chalcogenides as new photovoltaics. We chose those containing copper as a starting point due, in part, to the success of copper containing $CuIn_{1-x}Ga_xSe_2$ and Cu_2ZnSnS_4. Numerous ternary copper chalcogenides are known, and they adopt a wide variety of often complex crystal structure types (for example, see Ref. [3]). Among known materials, we chose $BaCu_2Se_2$ and $BaCu_2Te_2$ as cases for further study. These are but two of a large number of alkaline earth copper chalcogenides (which, interestingly, are known only for the alkaline earth Ba) [4–12]. Our selection of $BaCu_2Q_2$ (Q=Se, Te) was based on the three dimensional character of the covalent Cu–Se/Te framework, and our electronic structure calculations and those in the literature which indicated band gaps near 1 eV or larger [13]. For Q=S and Se, two structure-types can be stabilized: the orthorhombic $BaCu_2S_2$-type and tetragonal $ThCr_2Si_2$-type [4,5]. Only the $BaCu_2S_2$ structure has been reported for $BaCu_2Te_2$ [6,13].

Previous reports on $BaCu_2Se_2$ and $BaCu_2Te_2$ are limited to crystallographic studies [4–6], and, for the telluride, selected transport properties, and band structure calculated using the LMTO method [6,13]. Here we report the results of our investigation including experimental characterization as well as first principles calculations for both materials. Resistivity, carrier concentration inferred from Hall effect measurements, Hall mobility, Seebeck coefficient, thermal conductivity, and thermal expansion data are presented over a wide temperature range at and below 300 K for polycrystalline samples. Band structures, band gaps, and optical absorption from first principles calculations are also presented. Results of optical transmission and diffuse reflectance measurements are included for the selenide.

2. Materials and methods

$BaCu_2Se_2$ and $BaCu_2Te_2$ were synthesized from the elements (99.9% or higher purity), which were stored and handled in a helium filled glove box. Dendritic barium pieces, freshly reduced copper powder, and tellurium or selenium shot were combined in the ratio 1:2:2 (about 5 g total mass) and heated at 700 °C for 48 h in covered 5 cc alumina crucibles inside sealed, evacuated, silica ampoules. The products were ground and pelletized in air,

* Corresponding author.
E-mail address: McGuireMA@ornl.gov (M.A. McGuire).

0022-4596/$ - see front matter © 2011 Elsevier Inc. All rights reserved.
doi:10.1016/j.jssc.2011.08.021

sealed inside evacuated silica ampoules coated with carbon, and annealed at 675 °C for 48 h. For $BaCu_2Te_2$, a second grinding, pelletizing, and annealing was required (24 h at 675 °C). The intensity of the strongest unindexed reflections were less than 1% of the strongest main phase reflections, and the identities of the impurity phases are unclear. For transport properties measurements, dense samples were obtained by hot pressing in 3/8 in diameter graphite dies lined with graphite foil. A load of 300 kg was applied and the samples were heated at 500–600 °C for about 1 h. The resulting density of the telluride was 99% of the theoretical density. The hot-pressed selenide sample was 95% dense. Samples of both materials stored in air for many months showed no evident degradation. After about one year in air, the telluride showed some reaction/decomposition.

Powder x-ray diffraction data were collected using a PANalytical X'Pert Pro MPD with Cu$K\alpha$ radiation. An incident beam Johansson monochromator was used for collecting the data for Rietveld refinement at room temperature. For measurements below room temperature, the temperature was controlled with an Oxford Phenix closed cycle cryostat. Crystal structures were refined from PXRD data using the program FullProf [14]. Electrical resistivity, Hall effect, Seebeck coefficient, and thermal conductivity measurements were performed with a Quantum Design Physical Property Measurement System. With the measurement system and experimental arrangement used, parasitic radiative heat losses result in overestimated thermal conductivities at temperatures above about 200 K. Hall coefficients were determined from linear fits to transverse resistance data collected at applied magnetic fields ranging from −6 to 6 Tesla. Electrical and thermal contacts were made using Epotek H20E silver epoxy. For optical measurements, powdered samples were dispersed in a thin layers on silica cuvettes using acetone. Optical measurements were performed in transmission and diffuse reflectance modes with a Perkin Elmer Lambda 900 spectrophotometer and integrating sphere attachment.

The experimental, room temperature crystal structures were used to perform first principles calculations of the electronic structures and optical properties of $BaCu_2Se_2$ and $BaCu_2Te_2$. For this purpose, the recently developed functional of Tran and Blaha (denoted TB-mBJ here) was used [15]. This functional, which includes the kinetic energy density, greatly improves upon band gaps of many semiconductors and insulators as is needed for calculations of optical properties [15–17]. The calculations were performed using the general potential linearized augmented planewave method [18] as implemented in the WIEN2k code [19], using well converged basis sets including local orbitals for the semi-core states. Relativity was included in a scalar relativistic approximation for the valence states, while the core states were treated fully relativistically. The calculations were performed for stoichiometric, undoped materials.

3. Results and discussion

3.1. Crystal structure, electronic structure, alloying, and doping

Detailed descriptions of the coordination environments and bonding in $BaCu_2Q_2$ (Q=Se, Te) have been previously reported [5,6]. The orthorhombic structure is composed of a three dimensional Cu–Q network with Ba atoms residing in channels along the *b*-axis (Fig. 1a). Results of Rietveld refinement of powder x-ray diffraction patterns (Cu$K\alpha_1$ radiation) of the samples studied in this work are shown in Fig. 1b and c. Agreement factors and refined lattice constants are presented in Table 1. Other structural parameters are shown in Table 2. The results are in good agreement with previous reports from powder and single crystal x-ray diffraction

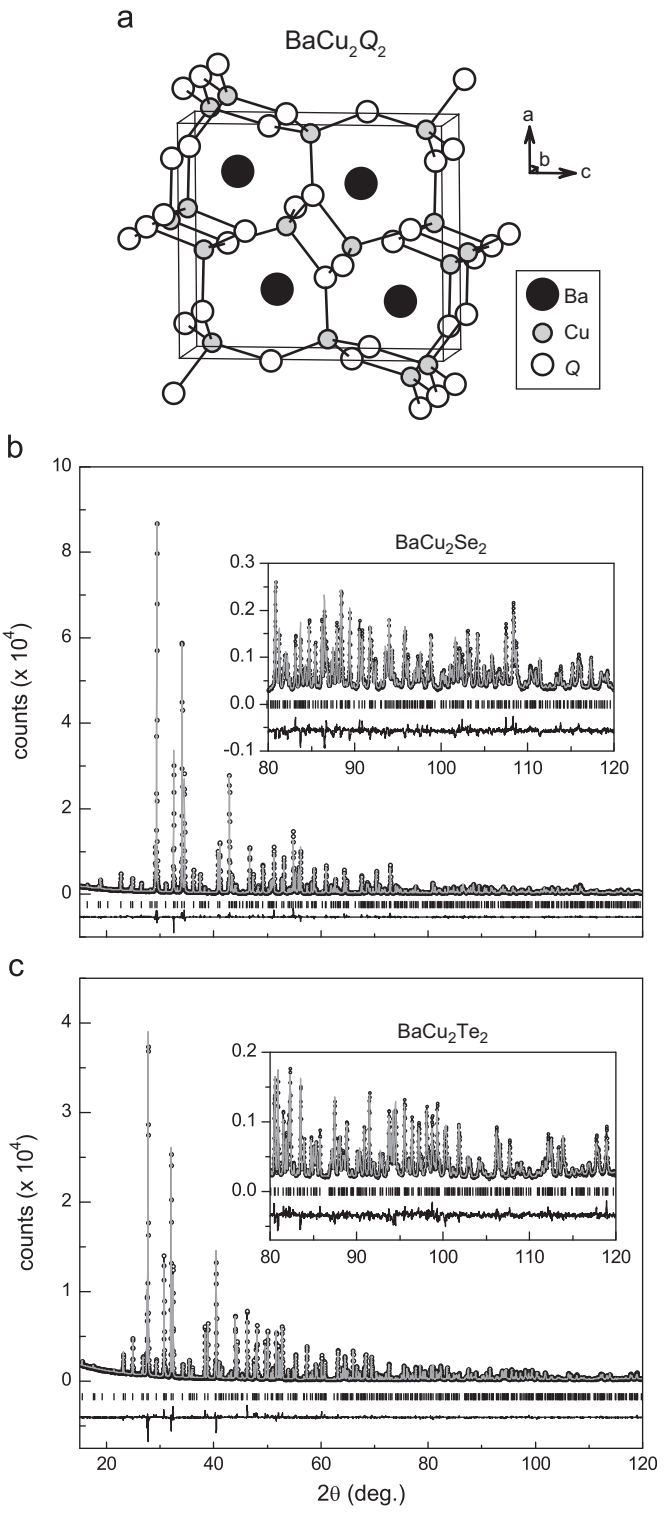

Fig. 1. (a) The crystal structure of orthorhombic $BaCu_2Se_2$ and $BaCu_2Te_2$ emphasizing the Cu–Te network. Powder diffraction data and Rietveld refinement for (b) $BaCu_2Se_2$ and (c) $BaCu_2Te_2$ samples studied in this work.

analysis of the telluride [6,13] and single crystal x-ray diffraction results for the selenide [4,5]. We attribute the smaller displacement parameters for the telluride to absorption effects, and note the ratios of displacement parameters between the different elements (which are relatively insensitive to absorption) agree well with the previous powder diffraction refinement [6]. The occupancy of the Cu sites was refined for both materials, and do not deviate significantly from unity with the possible exception of Cu_2 in $BaCu_2Se_2$. This may

Table 1
Unit cell parameters and agreement factors from Rietveld refinement of PXRD data collected at room temperature.

	$BaCu_2Se_2$	$BaCu_2Te_2$
a (Å)	9.59999(8)	10.12634(10)
b (Å)	4.21381(3)	4.45671(4)
c (Å)	10.78361(9)	11.47282(11)
V (Å^3)	436.224(6)	517.770(9)
R_p	5.1	5.7
R_{wp}	6.9	7.5
χ^2	5.1	3.9

Table 2
Refined atomic coordinates, isotropic displacement parameters (B_{iso}), and site occupancies (for Cu sites only) from PXRD data collected at room temperature shown in Fig. 1.

	x	y	z	B_{iso} (Å^2)	*occ.* (%)
$BaCu_2Se_2$					
Ba1	0.25909(10)	0.75	0.32260(9)	0.81(3)	–
Cu1	0.05542(22)	0.25	0.11008(22)	1.27(8)	99.2(6)
Cu2	0.42033(23)	0.75	0.04390(22)	1.25(8)	97.6(6)
Se1	0.48064(17)	0.25	0.17024(17)	0.76(4)	–
Se2	0.16055(17)	0.75	0.03819(16)	0.64(4)	–
$BaCu_2Te_2$					
Ba1	0.26007(16)	0.75	0.32257(16)	0.71(4)	–
Cu1	0.0551(4)	0.25	0.10783(39)	1.2(1)	98(1)
Cu2	0.42484(39)	0.75	0.04637(36)	1.2(1)	100(1)
Te1	0.48036(17)	0.25	0.17028(18)	0.53(4)	–
Te2	0.16173(17)	0.75	0.03915(16)	0.38(4)	–

indicate some Cu deficiency, but this cannot be conclusively determined from this powder x-ray diffraction data. Our results are consistent with the single crystal diffraction results of Assoud et al., which are expected to be more sensitive to site occupancies and found no evidence of Cu deficiency in the telluride [13]. No mention of Cu vacancies are made in the reported single crystal diffraction studies of the selenide [4,5].

Low temperature powder x-ray diffraction data were analyzed to determine the temperature dependence of the lattice parameters, and to investigate the possibility of structural phase transitions at low temperatures. No evidence of crystallographic phase transitions was observed between room temperature and 15 K. The lattice constants, determined by LeBail fits, are shown in Fig. 2. Similar thermal expansion behavior is observed in both materials.

The solid solution between the isostructural selenide and telluride was examined using synthesis techniques and temperatures similar to those employed for the endmembers. Analysis of powder x-ray diffraction patterns indicated that a $BaCu_2(Se_{1-x}Te_x)_2$ alloy with the orthorhombic $BaCu_2S_2$ structure type was successfully synthesized for $x=0.25$. The unit cell parameters were $a=9.7576(1)$ Å, $b=4.27397(5)$ Å, and $c=10.8694(1)$ Å. Attempts to synthesize samples with $x=0.5$ and 0.75 surprisingly were not successful; the products contain multiple complex, unidentified phases.

Since these materials form in heavily hole-doped states, electron doping was attempted to compensate for holes occurring in nominally stoichiometric materials. Lanthanum was chosen as a dopant to replace Ba, with the intent of restricting the dopant sites to the electropositive element position to minimize the effect on the electronically active Cu–Q framework. The transport properties of samples synthesized with 1% La were not significantly changed from the "undoped" materials. This suggests that either the substitution was not successful, or that La does not effectively introduce charge carriers.

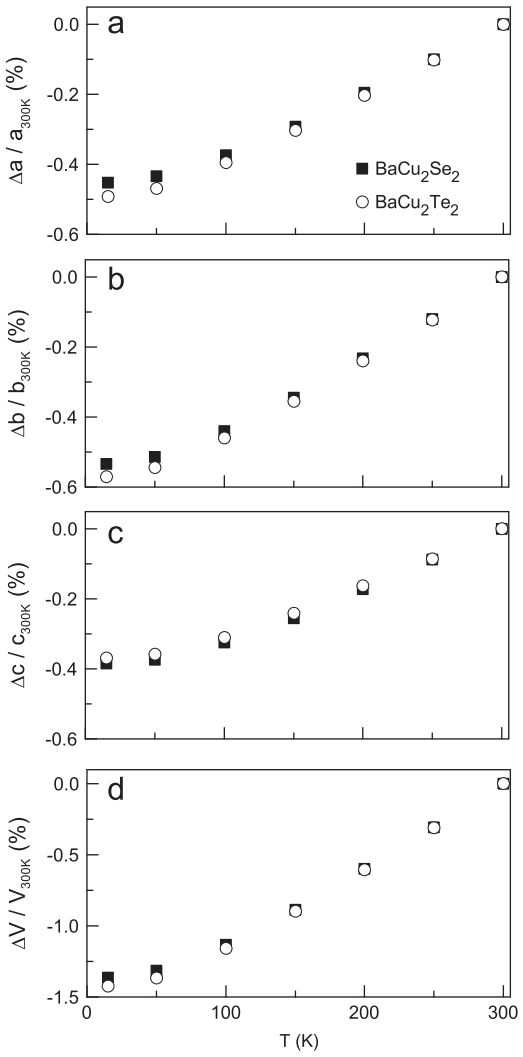

Fig. 2. Temperature dependence of the lattice parameters and cell volume V determined from refinement of powder x-ray diffraction data.

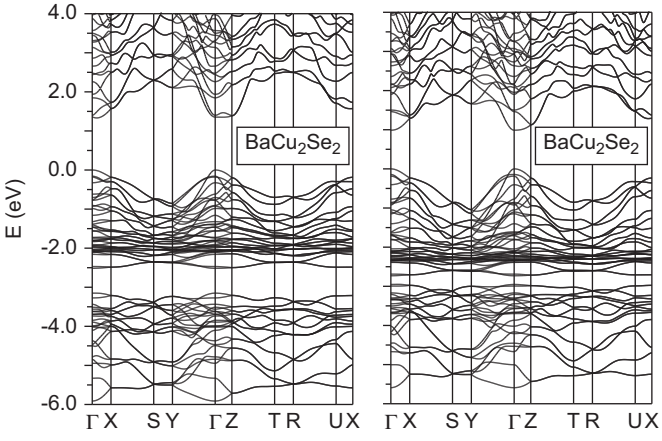

Fig. 3. Calculated band structures of orthorhombic $BaCu_2Se_2$ and $BaCu_2Te_2$ as obtained using the TB-mBJ functional with the experimental crystal structure.

The calculated band structures are shown in Fig. 3. The calculations yield quasi-direct or direct band gaps of 1.3 eV and 1.0 eV for $BaCu_2Se_2$ and $BaCu_2Te_2$, respectively. There are multiple heavy bands near both the valence and conduction band edges

and the gap is of charge transfer character between primarily chalcogen *p* derived valence band maxima and metal derived conduction bands. The Cu *d* states are hybridized in the valence bands, but the main Cu *d* character occurs below the valence band maxima between 1.5 eV and 2.5 eV binding energy. This binding energy may be underestimated as is the case for the Zn *d* states in ZnO with the TB-mBJ functional [17]. In any case, Cu occurs with a d^{10} configuration as might be anticipated from electron counting based on the chemical formulae and the main Cu *d* states are removed from the valence band edge. Dispersions of the bands at both the valence and conduction band edges are rather anisotropic, with stronger dispersions along the $\Gamma-Y$ than the other crystallographic directions. This corresponds to the direction of "channels" along the *b*-axis in the crystal structure (Fig. 1). This implies anisotropic transport properties, especially anisotropy in the electrical conductivity.

3.2. Electrical and thermal transport properties

Measured transport properties of $BaCu_2Se_2$ and $BaCu_2Te_2$ are presented in Figs. 4 and 5. The measurements were performed on dense, hot-pressed, polycrystalline samples. Values of the transport properties near room temperature are summarized in Table 3. Both materials are *p*-type, as indicated by positive Hall and Seebeck coefficients.

The properties of $BaCu_2Te_2$ will be addressed first. The carrier concentration (n_H) inferred from Hall effect measurements for

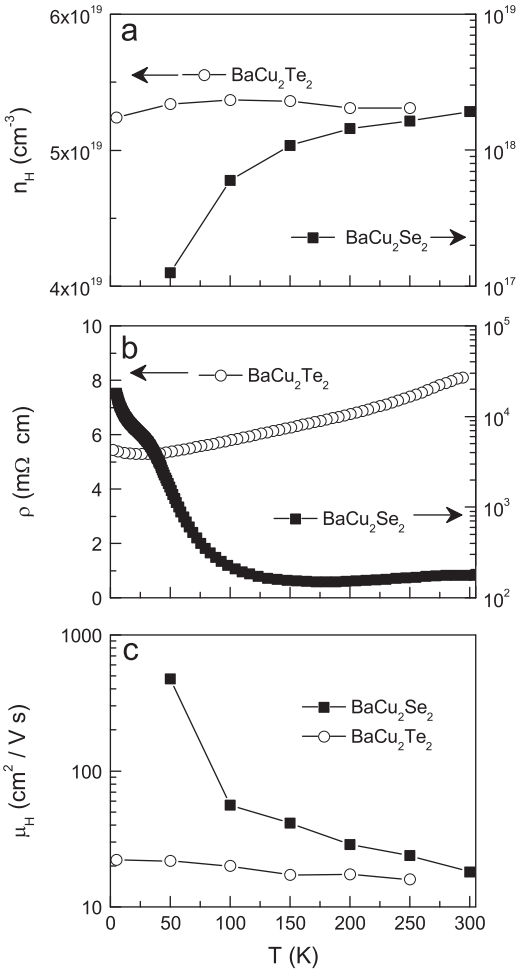

Fig. 4. Temperature dependence of electrical transport properties: (a) carrier concentration inferred from Hall effect measurements, (b) electrical resistivity, and (c) calculated Hall mobility determined from data in (a) and (b).

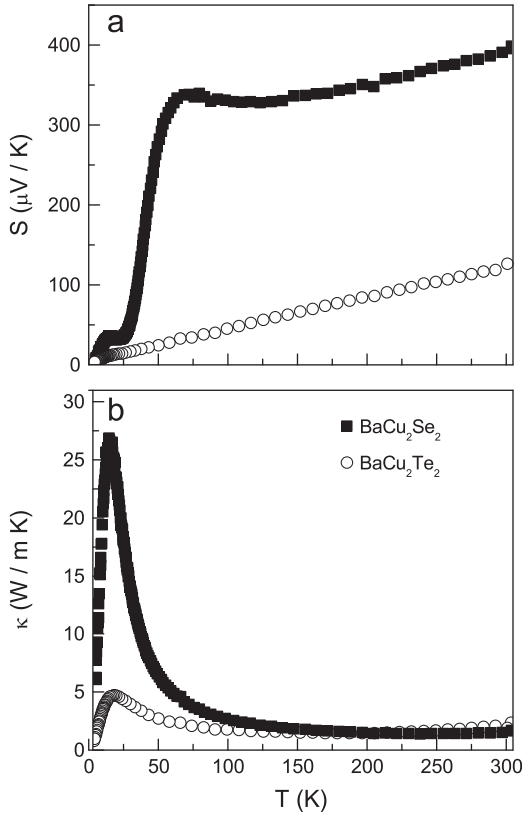

Fig. 5. Temperature dependence of thermal transport properties: (a) Seebeck coefficient and (b) thermal conductivity.

Table 3
Transport properties of $BaCu_2Se_2$ and $BaCu_2Te_2$ near room temperature.

	$BaCu_2Se_2$	$BaCu_2Te_2$
n_H (10^{18} cm^{-3})	1.9	53
ρ (mΩ cm)	181	8.1
μ_H(cm^2 V^{-1} s^{-1})	18	15
S (μV K^{-1})	390	127
κ[a] (W m^{-1} K^{-1})	1.5	2.0

[a] Expected to be overestimated due to radiative heat losses. Both materials have $\kappa = 1.5$ W m^{-1} K^{-1} at 200 K, where radiation corrections are negligible.

$BaCu_2Te_2$ (Fig. 4a) is nearly temperature independent from 5 to 250 K, and is expected to remain near the same value at room temperature. The resistivity (ρ) decreases upon cooling, but remains relatively high at 2 K. The Seebeck coefficient increases linearly with temperature and attains modestly high values at room temperature. The Hall mobility (μ_H) ranges from $\sim$15 to 20 cm^2 V^{-1} s^{-1} over the temperature range investigated (Fig. 4c). These behaviors are typical of a heavily doped (degenerate) semiconductor. The thermal conductivity (κ) is shown in Fig. 5b, and is dominated by the lattice contribution at all temperatures. The maximum electronic contribution is about 0.1 W m^{-1} K^{-1}. The low temperature peak in κ, typical of crystalline materials, is suppressed in $BaCu_2Te_2$. This is likely due to strong electron phonon scattering in this material, and the defects responsible for the naturally high doping level. The transport behavior for $BaCu_2Te_2$ shown in Figs. 4 and 5 and Table 3 are similar to those reported by Wang and DiSalvo [6], who found at room temperature $S = 88.3$ μV K^{-1}, $\rho = 7.959$ mΩ cm, and $\kappa = 2.25$ W m^{-1} K^{-1}. Discrepancies may be attributed to differences in doping/defect levels, and the densities of the samples which were prepared and sintered under different conditions. In particular, the

lower values of both S and ρ reported in [6] may indicate a higher carrier concentration in that sample, relative to the sample studied in this work. We also note that the resistivity anomaly observed near 65 K in Ref. [6] was not observed here.

The electrical and thermal transport behaviors of $BaCu_2Se_2$ are significantly different than those of the telluride. This is primarily due to the lower carrier concentration that is found in the nominally stoichiometric samples (Fig. 4a). This results in an electrical resistivity that is more than one order of magnitude higher than that of $BaCu_2Te_2$ (Fig. 4b), though the mobilities near room temperature are similar (Fig. 4c). The lower carrier concentration in the selenide also leads to significant enhancement of the Seebeck coefficient (Fig. 5a), and the low temperature thermal conductivity (Fig. 5b). In contrast to the telluride, the inferred carrier concentration, resistivity, and Seebeck coefficient of $BaCu_2Se_2$ show strong temperature dependence. Upon warming to about 100 K, n_H and S increase rapidly while ρ decreases sharply. This is consistent with the activation of acceptor sites increasing the concentration of holes in the valence band. The unusual behavior of S and ρ below about 50 K may indicate the presence of multiple acceptors with different activation energies. Analysis of the lowest temperature resistivity data gives an activation energy as low as 0.2 meV. An activation energy near 7 meV is found at intermediate temperatures ($40\ K < T < 100\ K$) Above 150 K, n_H changes more slowly, and ρ and S show heavily doped semiconductor behavior, qualitatively similar to $BaCu_2Te_2$.

The doping dependencies of the single crystal Seebeck coefficient of p-type $BaCu_2Se_2$ and $BaCu_2Te_2$ were calculated within the constant scattering time approximation (CSTA) using the first principles band structures (Fig. 3). This was done with the BoltzTraP code [20]. The CSTA consists of the approximation that the scattering rate is energy independent at fixed doping and temperature but makes no assumptions about its temperature or doping dependence. It allows for a parameter free calculation of the thermopower from the band structure and has been applied to a variety of thermoelectric materials [21–24]. The calculated S are given in Fig. 6a and b for $BaCu_2Se_2$ and $BaCu_2Te_2$, respectively. Both compounds show high Seebeck coefficients at moderate to high doping levels. For carrier concentrations above about 5×10^{19} cm^{-3}, S shows increased curvature, deviating from behavior expected from a single parabolic band. The non-parabolic nature of the bands is also evidenced by the anisotropy in S, since an anisotropic but parabolic band gives an isotropic S in the CSTA.

The experimental data shown in Table 3 agree reasonably well with the calculated Seebeck coefficients shown in Fig. 6. The measured data from the polycrystalline samples are closest to values calculated for the b-direction. In a polycrystalline sample with randomly oriented grains, the measured thermopower corresponds to a weighted, directional average of the single crystal S, with the direction of largest electrical conductivity having higher weights than others. While the conductivity cannot be obtained without knowledge of the scattering rates, the anisotropies, σ_{yy}/σ_{xx} and σ_{yy}/σ_{zz} can be calculated within the CSTA, with the additional assumption of isotropic scattering rates. As shown in Fig. 6c, the conductivity is expected to be highly anisotropic. The materials have the highest conductivity along the b-direction, which corresponds to the axis of the "channels" in the crystal structure (Fig. 1). This is likely related to the closer agreement of the measured data to the calculated b-axis Seebeck coefficient.

Since partial occupation of copper sites often occur in these types of materials [10–12,25,26], Cu vacancies are good candidates for the defects responsible for the hole doping in these compounds. For this reason, density functional calculations within the generalized gradient approximation [27] (GGA) were carried out to compare the formation energies of Cu vacancies in the selenide and telluride. Absolute formation energies of Cu vacancies were not determined because the Cu chemical potential is unknown. Instead, the difference in Cu vacancy formation energies for the selenide and telluride was examined. The results show that the formation energy of a Cu vacancy in $BaCu_2Se_2$ is higher than that in $BaCu_2Te_2$ by 0.05 eV, assuming the Fermi level at the valence band maximum (VBM) and the same Cu chemical potential in both compounds. However, underestimation of the Cu 3d band binding energy in the GGA calculation should result in an artificially higher VBM (due to the hybridization between the VBM states and the Cu 3d states), which further leads to an artificially lower formation energy for Cu vacancy if the Fermi level is fixed at the calculated VBM. This error should be larger in $BaCu_2Se_2$ since the VBM in $BaCu_2Se_2$ is lower than in $BaCu_2Te_2$, causing a stronger repulsion between the VBM and the Cu 3d states in $BaCu_2Se_2$. As a result, the formation energy (at VBM) of a Cu vacancy in $BaCu_2Se_2$ relative to that in $BaCu_2Te_2$ should be higher than the GGA result of 0.05 eV. This is consistent with the observed lower carrier concentration in the nominally stoichiometric selenide, and suggests that Cu vacancies may be at least partly responsible for the unintentional doping in these compounds. Finally, at the annealing temperature of 675 °C, a Cu

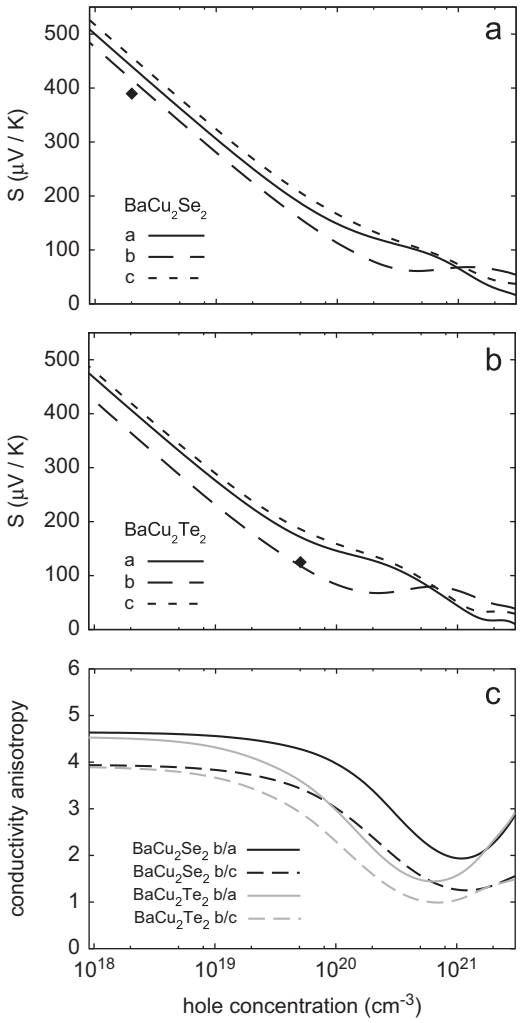

Fig. 6. Calculated Seebeck coefficient for (a) $BaCu_2Se_2$ and (b) $BaCu_2Te_2$ as a function of hole concentration at 300 K. Results for transport along the three crystallographic axes are shown. The black diamonds correspond to the experimental Seebeck coefficient and carrier concentration data from Table 3. (c) Calculated anisotropy of the electrical conductivity at 300 K.

vacancy formation energy difference of 0.2–0.3 eV could account for the difference in observed hole densities.

3.3. Optical properties and potential for energy applications

The formally charge balanced compositions of $BaCu_2Se_2$ and $BaCu_2Te_2$ are consistent with their semiconductor like transport properties. Density functional theory calculations suggest a band gap near 1.3 eV for the selenide, and 1 eV for the telluride. In powder form, the telluride is black and the selenide is very dark red, consistent with band gaps less than about 2 eV. To determine the optical band gaps, diffuse reflectance and transmission spectra were collected from thin layers of dispersed powders over the energy range of 0.5–6 eV. The results for $BaCu_2Se_2$ are shown in Fig. 7, and reveal an optical transition near 1.8 eV, consistent with the dark red color of the material. No similar features were observed in the optical spectra from $BaCu_2Te_2$. This may be due to the smaller penetration depth resulting from the higher carrier concentration in the telluride. An instrumental anomaly occurring near 1.4 eV (associated with switching between photon detectors) could mask a weak transition near this energy.

The optical properties were calculated with electric dipole matrix elements using the optical package of the WIEN2k code. The resulting directionally averaged absorption coefficients are shown in Fig. 8. The onset of strong absorption in these compounds is higher than the fundamental band gaps, even though the gaps are direct. This is a consequence of the matrix elements. The onset of strong absorption in these compounds is at $\sim$2 eV, which is close in energy to the transition observed in the optical measurements on the selenide shown in Fig. 7. The calculated absorption coefficient of the telluride is higher than that of the selenide in the visible region as may be expected from the trend in the band gaps, with the smaller gap leading to increased absorption. The weak absorption onset calculated for these materials, together with their high carrier concentrations in nominally stoichiometric samples, relatively low mobility, and resistance to our preliminary attempts at doping, do not lead us to expect good photovoltaic performance.

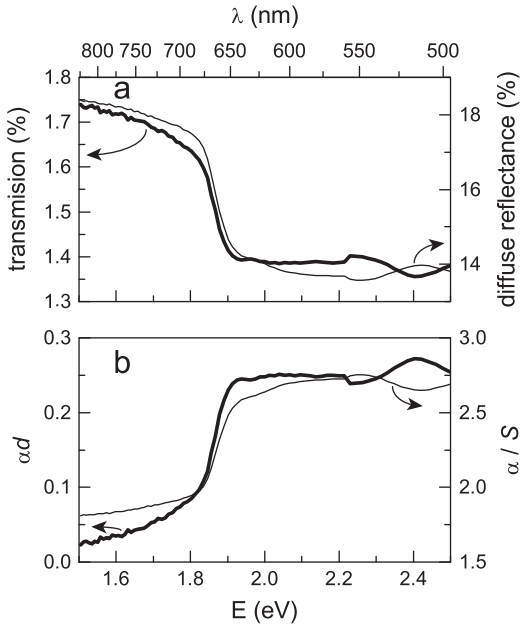

Fig. 7. Optical properties of $BaCu_2Se_2$ around the optical transition near 1.8 eV: (a) Measured transmission T and diffuse reflectance R data and (b) αd ($=-\ln(T/T_0)$) from transmission data and α/S ($=(1-R)^2/2R$) from Kubelka–Munk transform of diffuse reflectance data.

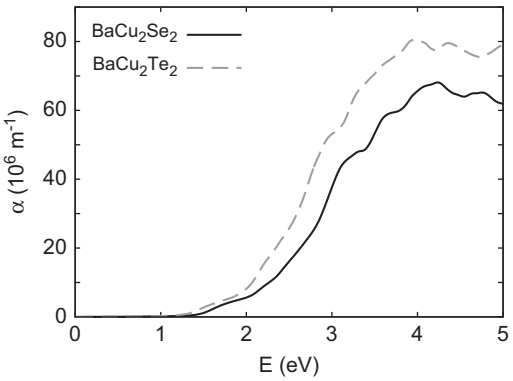

Fig. 8. Calculated directionally averaged absorption coefficients of $BaCu_2Se_2$ and $BaCu_2Te_2$ as obtained using the TB-mBJ functional with the experimental crystal structure. Note that due to matrix element effects the onset of strong absorption is higher than the fundamental band gaps.

The thermoelectric performance of $BaCu_2Te_2$ [6], as well as several related materials [10,13,28], has been explored. No promising behavior has been reported, and our results follow this trend. Good thermoelectric materials require low thermal conductivity, low electrical resistivity, and high Seebeck coefficient to achieve a large figure of merit $zT = S^2T/\rho\kappa$, a measure of their efficiency [29]. Over the temperature ranges investigated, low zT values in these materials are primarily due to high electrical resistivities. Better performance may be possible if carrier concentrations could be controlled. Our calculations also show that the resistivity should be lowest along the b-direction (Fig. 6c), indicating the best performance would require single crystals or oriented polycrystalline materials.

4. Conclusions

Results of our experimental and theoretical investigation of the transport and optical properties of orthorhombic $BaCu_2Se_2$ and $BaCu_2Te_2$ have been reported. The samples behave as heavily doped semiconductors, with room temperature Hall mobilities near 15 $cm^2\ V^{-1}\ s^{-1}$. Activated resistivity behavior was observed in the selenide, while the telluride showed degenerate semiconductor or poor metal behavior due to its higher carrier concentration. At low temperatures, the telluride has a significantly lower thermal conductivity than the selenide. This is attributed to the higher carrier concentration in the telluride, and the larger mass of Te relative to Se. Optical characterization was hindered by the polycrystalline nature of the materials, and by high absorption; however, an optical transition was observed in the selenide near 1.8 eV in both diffuse reflection and transmission experiments. This energy is close to the strong onset of absorption predicted by first principles calculations. These calculations indicate band gaps near 1.3 eV for the selenide and 1 eV for the telluride. Although the gaps are direct or nearly direct, matrix elements lead to weak absorption below about 2 eV. Experimental values of the Seebeck coefficient at room temperature are in reasonable agreement with those calculated from the band structure using the constant scattering time approximation. Based on the results of our optical and transport studies, these materials as prepared are not expected to perform well in photovoltaic or thermoelectric applications.

Acknowledgments

Research sponsored by the Laboratory Directed Research and Development Program of Oak Ridge National Laboratory, managed

by UT-Battelle, LLC, for the U.S. Department of Energy (experimental work and optical properties calculations) and the U.S. Department of Energy through the Office of Science, Materials Sciences and Engineering Division (electronic structure calculations).

References

[1] I. Repins, M. Contreras, M. Romero, Y.F. Yan, W. Metzger, J. Li, S. Johnston, B. Egaas, C. DeHart, J. Scharf, B.E. McCandless, R. Noufi, in: 33rd IEEE Photovoltaic Specialists Conference, vols. 1–4, 2008, p. 1127.
[2] D.B. Mitzi, O. Gunawan, T.K. Todorov, K. Wang, S. Guha, Sol. Energy Mater. Sol. Cells 95 (2011) 1421.
[3] H. Boller, J. Alloys Compd. 442 (2007) 3.
[4] J. Huster, W. Bronger, Z. Anorg. Allg. Chem. 625 (1999) 2033.
[5] J.E. Iglesias, K.E. Pachali, H. Steinfink, J. Solid State Chem. 9 (1974) 6.
[6] Y.C. Wang, F.J. DiSalvo, J. Solid State Chem. 156 (2001) 44.
[7] J. Iglesias, K. Pachali, H. Steinfink, Mater. Res. Bull. 7 (1972) 1247.
[8] J. Chang, H. Hong, G. Lee, Y. Wang, Mater. Res. Bull. 25 (1990) 863.
[9] Y. Cui, A. Assoud, J. Xu, H. Kleinke, Inorg. Chem. 46 (2007) 1215.
[10] A. Assoud, S. Thomas, B. Sutherland, H. Zhang, T. Tritt, H. Kleinke, Chem. Mater. 18 (2006) 3866.
[11] O. Mayasree, Y. Cui, A. Assoud, H. Kleinke, Inorg. Chem. 49 (2010) 6518.
[12] B. Kuropatwa, Y. Cui, A. Assoud, H. Kleinke, Chem. Mater. 21 (2009) 88.
[13] A. Assoud, Y. Cui, S. Thomas, B. Sutherland, H. Kleinke, J. Solid State Chem. 181 (2008) 2024.
[14] J. Rodriguez-Carvajal, FullProf Suite 2005, version 3.30, June 2005, ILL.
[15] F. Tran, P. Blaha, Phys. Rev. Lett. 102 (2009) 226401.
[16] D.J. Singh, Phys. Rev. B 82 (2010) 155145.
[17] D.J. Singh, Phys. Rev. B 82 (2010) 205102.
[18] D.J. Singh, L. Nordstrom, Planewaves, Pseudopotentials and the LAPW Method, second ed., Springer Verlag, Berlin, 2006.
[19] P. Blaha, K. Schwarz, G. Madsen, D. Kvasnicka, J. Luitz, WIEN2k, An Augmented Plane Wave + Local Orbitals Program for Calculating Crystal Properties, Tech. Univ., Wien, Austria, 2001.
[20] G.K.H. Madsen, D.J. Singh, Comput. Phys. Commun. 175 (2006) 67–71.
[21] D.J. Singh, I.I. Mazin, Phys. Rev. B 56 (1997) R1650.
[22] G.K.H. Madsen, K. Schwarz, P. Blaha, D.J. Singh, Phys. Rev. B 68 (2003) 125212.
[23] L. Zhang, D.J. Singh, Phys. Rev. B 80 (2009) 075117.
[24] D.J. Singh, Phys. Rev. B 81 (2010) 195217.
[25] G. Sorokin, G. Idrichan, Z. Sorokina, Neorg. Mater. 11 (1975) 1357.
[26] B. Mansour, B. Farag, S. Khodier, Thin Solid Films 247 (1997) 112.
[27] J. Perdew, K. Burke, M. Ernzerhof, Phys. Rev. Lett. 77 (1996) 3865.
[28] A. Assoud, N. Soheilnia, H. Kleinke, Chem. Mater. 17 (2006) 2255.
[29] A. Ioffe, Semiconductor Thermoelements and Thermoelectric Cooling, Infosearch Ltd., London, 1957.